MEGAHERTZ MONOCRYSTALLINE OPTOMECHANICAL RESONATORS WITH MINIMAL DISSIPATION

Garrett D. Cole[1,2], Ignacio Wilson-Rae[3], Michael R. Vanner[1,4], Simon Gröblacher[1,4], Johannes Pohl[5], Martin Zorn[5], Markus Weyers[5], Achim Peters[6], and Markus Aspelmeyer[4]
[1]Institute for Quantum Optics and Quantum Information, Austrian Academy of Sciences
[2]Center for Micro and Nano Structures, Vienna University of Technology
[3]Department of Physics, Technical University Munich
[4]Faculty of Physics, University of Vienna
[5]Ferdinand-Braun-Institute, Berlin
[6]Institute of Physics, Humboldt University Berlin

ABSTRACT

We present detailed experimental and theoretical results for novel micro-optomechanical resonators, representing a significant improvement in the performance of such structures. These devices exhibit eigenfrequencies (f_r) approaching 4 MHz, reflectivities exceeding 99.98% at 1064 nm, and mechanical quality factors (Q) of 0.8×10^5 (measured at 20 K and 2.5×10^{-7} millibar pressure); yielding a $Q{\cdot}f_r$ product of 3.1×10^{11} Hz, while enabling a finesse of approximately 20,000 when used as an end mirror in an impedance-matched Fabry-Pérot optical cavity. These results represent a breakthrough in the development of optomechanical devices applicable to the emerging field of quantum optomechanics.

INTRODUCTION

The overarching goal of the rapidly expanding field of quantum optomechanics [1] is to combine the concepts of quantum optics with optomechanical coupling in order to generate and detect quantum states of MEMS/NEMS [2,3]. Recent theoretical analysis [4,5] predicts that resonators of sufficient acoustic and optical quality are capable of ground-state cooling by utilizing a radiation-pressure-based laser cooling process [6,7]. Currently, the best results from our group involve cooling the mechanical mode of a 1 MHz oscillator (Q of 30,000) to a phonon occupation near 30, corresponding to an effective mode temperature of 1.3 mK [8]. The rate of rethermalization (i.e. coupling to the external environment) is the primary hurdle that prevents laser cooling to the vibrational ground state. In this light, we present optomechanical resonators utilizing a novel free-free geometry capable of significantly reduced mechanical dissipation.

With enhanced coupling between photons and vibrational modes, high-performance optomechanical devices enable new and unexpected applications, ranging from metrology (e.g. mechanical frequency combs), sensing (e.g. single-molecule detection), and actuation (e.g. optically-driven switches). Moreover, the interplay between light and MEMS/NEMS facilitates the preparation of mechanical quantum states. Entering the quantum regime will allow for novel opportunities, ranging from fundamental scientific studies to applied efforts, including sensing at or beyond the quantum limit, as well as novel approaches to quantum information processing where mechanical states may enable the storage and coherent manipulation of quantum information.

EPITAXIAL LAYER STRUCTURE

To simultaneously achieve high-Q and high-reflectivity, we fabricate our optomechanical resonators directly from an epitaxial $Al_xGa_{1-x}As$ Bragg reflector. Compared with dielectric mirrors, the use of a monocrystalline heterostructure gives rise to a significant increase in Q, while simultaneously exhibiting near unity reflectivity [9]. In this implementation, the use of compound semiconductor materials such as GaAs and related alloys allows for the generation of arbitrary stacks of high-index-contrast materials (thus capable of high reflectivity for a given stack thickness) with reduced levels of mechanical dissipation as compared with the amorphous constituents of dielectric mirrors.

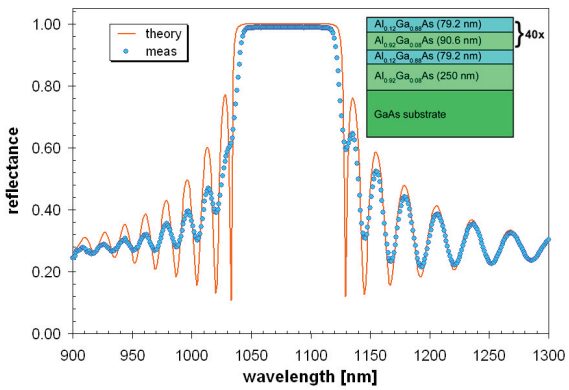

Figure 1: Theoretical and experimental reflectance spectrum for a 41 period single-crystal Bragg reflector (including etch stop). Note that this measurement was made on wafer. As shown in the inset, the epitaxial structure consists of alternating quarter wave $Al_{0.12}Ga_{0.88}As$ and $Al_{0.92}Ga_{0.08}As$ layers, with a total thickness of nearly 7 µm.

As shown in Fig. 1, the epitaxial materials structure consists of alternating quarter-wave $Al_{0.12}Ga_{0.88}As$ (high index) and $Al_{0.92}Ga_{0.08}As$ (low index) layers, followed by an approximately 250-nm thick $Al_{0.92}Ga_{0.08}As$ etch-protection layer, grown on a

crystalline GaAs substrate. In this design, the thick high-aluminum-content layer below the Bragg stack is included to protect the bottom of the mirror during the undercut etching process. The peak reflectivity of the distributed Bragg reflector (DBR) is designed to be at 1064 nm at cryogenic temperature; thus, the wavelength of maximum reflectivity at room temperature is red-shifted to 1078 nm to compensate for thermo-optic effects upon cooling. The refractive index of the ternary compounds at cryogenic temperatures is estimated using the modified Afromowitz model developed in [10]. Assuming no absorption and atomically smooth interfaces, the maximum achievable reflectivity (after stripping the protective $Al_{0.92}Ga_{0.08}As$ layer and with air cladding top and bottom) is calculated to be 99.999% at 1064 nm for temperatures below 20 K.

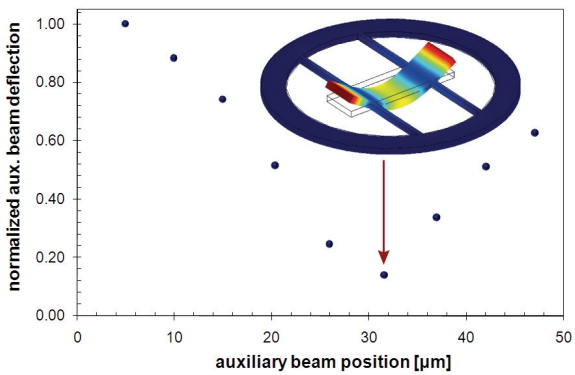

Figure 2: Design of the free-free resonator. The plot displays the integrated displacement of the auxiliary beams as a function of attachment position. Inset: eigenfrequency simulation of the ideal resonator geometry.

RESONATOR DESIGN

For the novel optomechanical resonators discussed in this manuscript, we utilize a free-free geometry [11,12] to minimize clamping loss. In this design the mirror geometry has been engineered in order to reduce mechanical coupling to the environment by attaching the auxiliary support beams at the nodal points of the fundamental mode of the central beam, greatly reducing dissipation induced by phonon tunneling [13]. Finite element modeling (FEM) is used to determine the optimum contact position by investigating the total deflection of the auxiliary beams, as in Fig. 2. In order to experimentally verify the ideal resonator layout, a variety of geometries have been included on chip. Here, the attachment points of the auxiliary beams are varied over the full span of the mirror, allowing for unambiguous identification of the fundamental flexural mode of the central resonator (hereinafter referred to as the 'free-free' mode) as well as an in-depth investigation on the effects of the auxiliary beam position on the mechanical dissipation of the devices.

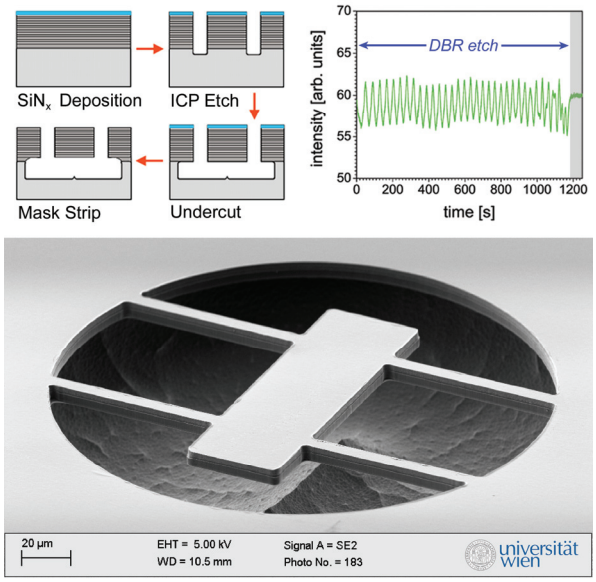

Figure 3: (Top) Cross-sectional schematic of the monocrystalline optomechanical resonator process flow, as well as an example plot of the laser endpoint detector trace generated during the DBR etch process. (Bottom) Scanning electron micrograph of a completed resonator structure.

MICROFABRICATION PROCEDURE

Fabrication of the resonators begins with the deposition of a SiN_x hard mask via plasma enhanced chemical vapor deposition. Next, the device geometry is patterned lithographically using a standard positive photoresist; this pattern is then transferred into the SiN_x via plasma etching with SF_6. Definition of the resonator geometry in the $Al_xGa_{1-x}As$ epilayers relies on an inductively coupled plasma reactive ion etch through the mirror stack using $SiCl_4/N_2$, with masking provided by the resist/SiN_x. A laser endpoint detector is utilized to ensure repeatability of the etch depth. Note that for the 40-period DBR samples, the total etch depth exceeds 7 µm.

To undercut the resonators, a buffered citric acid solution is utilized [14]. This selective wet etching process allows for the removal of the binary GaAs—in this case the substrate—over the low-aluminum content ternary $Al_{0.12}Ga_{0.88}As$ layers with excellent selectivity [15]. During the undercutting process, the SiN_x coating protects the top surface of the mirror, while the thick $Al_{0.92}Ga_{0.08}As$ layer protects the bottom, ensuring minimal surface roughness and maximum reflectivity. To complete the fabrication sequence, the protective SiN_x and $Al_{0.92}Ga_{0.08}As$ layers are removed via a combination of dry and wet etching. First an SF_6 reactive ion etch is utilized to thin the SiN_x layer. Note that this etch process is also monitored via laser endpoint detection in order to avoid exposure of the DBR surface to the plasma.

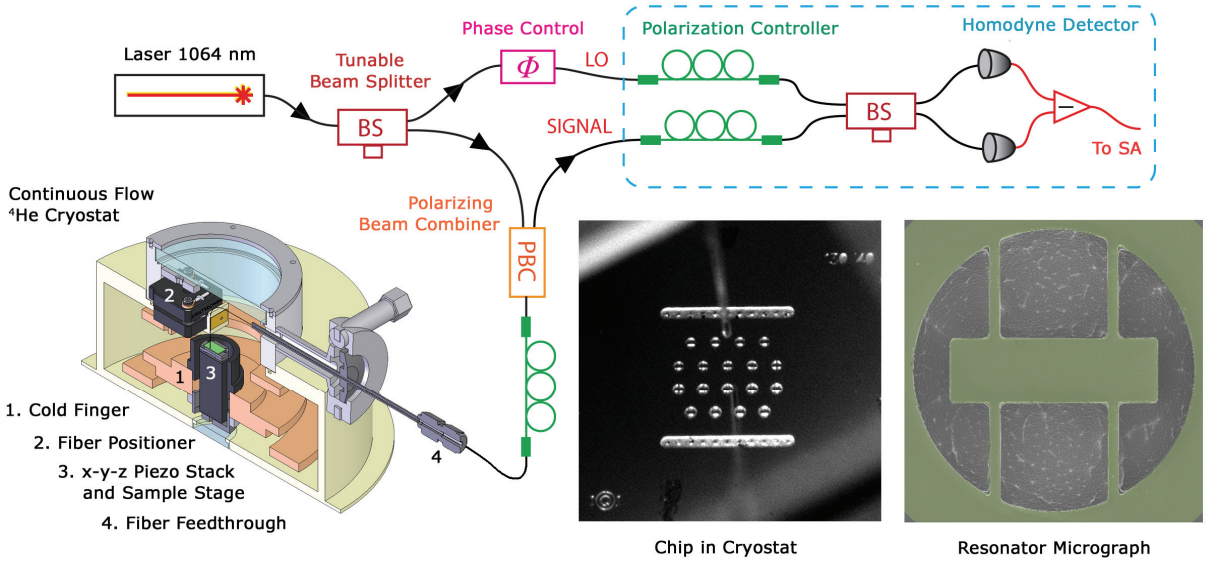

Figure 4: Schematic of our custom-built optical fiber interferometer. The sample chip is placed in a continuous flow ^{4}He cryostat and driven with a high-frequency piezo disc. The frequency response of the mechanical resonator is detected by optical homodyne interferometry, providing a low-noise readout of the noise power spectrum. This system allows for temperature dependent measurements from 300 K to 20 K, and from atmospheric pressure to vacuum levels of 2.5×10^{-7} millibar. The micrograph in the lower right also includes an overlay of the CAD model used in the FEM solver (color only).

Finally, the remaining nitride film and the backside $Al_{0.92}Ga_{0.08}As$ etch protection layer are removed with a dilute hydrofluoric acid solution. Given the large spring constant of these structures (roughly 2000 N/m), we observe no adverse effects arising from surface tension forces and the completed resonators are simply allowed to air-dry after rinsing. A scanning electron micrograph highlighting a free-standing resonator is included in Fig. 3.

CRYO FIBER INTERFEROMETER

To characterize the frequency response of our microresonators, we utilize a custom-built optical fiber interferometer featuring a continuous flow ^{4}He cryostat as the sample chamber (Fig. 4). The turbo-pumped cryostat enables interrogation from room temperature (RT) to 20 K, and from atmospheric pressure to vacuum levels of 2.5×10^{-7} millibar. We detect the phase fluctuations of the reflected field via optical homodyne interferometry, which provides a high-sensitivity readout of the resonator position. The eigenmodes of the resonator are excited by driving a high-frequency (10 MHz) piezo disc soldered to a copper stage in thermal contact with the cold finger.

In our experiments, the mechanical dissipation is characterized by measuring the position noise power spectrum (NPS), whereby, knowledge of the mechanical frequency response, or additionally, the decay of a ringing structure, provides the damping rate of the system. We obtain the mechanical NPS by measuring the phase fluctuations of the optical field reflected from the driven resonator. In this setup we utilize two options for driving the micromechanics: 1) by applying broadband white noise to the piezo disc for extraction of the mechanical frequency spectrum, and 2) by exciting a desired mode resonantly with a sinusoidal voltage input and then recording the free-ringdown of the structure. The incident optical field is launched with circular polarization from a cleaved fiber tip (our cryostat employs a fiber-optic vacuum feedthrough system similar to that described in ref [16]) brought close to the surface of the mechanical resonator. The injected signal is then retro-reflected, collected by the fiber, and separated using an in-line polarizing beam combiner. The phase fluctuations of this field are measured with a fiber based homodyne detection scheme and the resonator frequency response is recorded directly with a low-noise spectrum analyzer. Additionally, the decay of a resonantly driven actuator is recorded in a single shot (free-ringdown) on a high-speed oscilloscope for an accurate determination of the mechanical Q value.

In contrast to similar interferometers demonstrated previously, where the signal is seen as interference between prompt reflection at the fiber tip and the reflection from the cantilever [17], here, we employ a homodyne detection scheme. Such a scheme leads to a number of advantages: it dramatically relaxes the requirement for tip positioning above the cantilever, it provides a means to achieve high signal to noise for weak optical probes thus minimizing radiation pressure perturbations, and finally, it is less sensitive to optical intensity fluctuations that may be present in the test system.

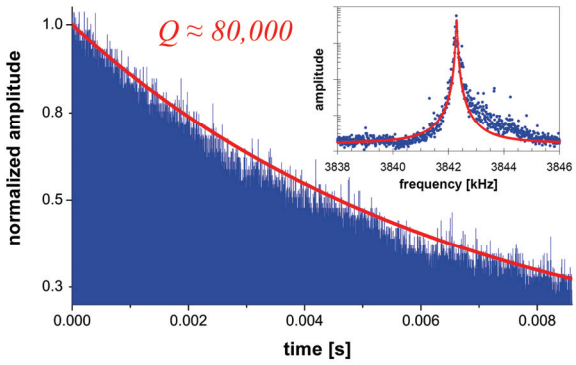

Figure 5: Experimental ringdown and accompanying exponential fit for the free-free resonance of a 100×50 μm² resonator fabricated from a 40-period mirror stack and measured at 20 K and 2.5×10⁻⁷ millibar. The exponential decay rate (τ = 0.007 s) yields a Q value of ~80,000. The inset displays the frequency response of the resonator when driven with a white noise signal along with a Lorentzian fit.

OPTOMECHANICAL PROPERTIES

Mirror Reflectivity

Finesse measurements have been undertaken for both 32 and 40 period mirror structures using a custom built optical cavity consisting of a curved input mirror (with an estimated amplitude reflectivity of 0.999948), a 1 mm air gap, and a flat end mirror consisting of a cleaved sample of the epitaxial DBR material (tested on wafer). The 32-period mirror appears to be limited to reflectivity values below 99.94%, corresponding to a finesse value of 1.0×10^3. Increasing the period count to 40 results in an enhanced amplitude reflectivity, in this case exceeding 99.98% (extracted from a finesse value of 2.6×10^4). This level of reflectivity is comparable with that measured in our previous optomechanical resonators utilizing a high performance multilayer dielectric coating (comprising a 36 period Ta_2O_5/SiO_2 mirror stack with a nominal reflectivity of 99.991% [8]). Furthermore, AFM measurements of the 32-period mirror surface yield an average surface roughness below 2 Å over a 10 μm × 10 μm scan area, demonstrating the extremely high material quality produced via epitaxial growth techniques.

Mechanical Dissipation

As expected, the RT mechanical quality factor suffers from limitations imposed by thermoelastic damping (TED). In this case the dissipation level is fairly well described by the classic Zener model [18]. At 300 K the typical quality factors for these devices range from 4.4×10^3 to 6.7×10^3, depending on the specifics of the device geometry and resulting operating frequency (between 2 and 4 MHz for the structures investigated here). The calculated Q values predict a similar order of magnitude, ranging from 3.6×10^3 to 4.6×10^3 respectively. Upon cooling to cryogenic temperatures, TED is significantly reduced and Q increases dramatically, reaching a current maximum value of 0.8×10^5 at 3.84 MHz for a 100×50 μm² central resonator (Fig. 5); yielding a $Q{\cdot}f_r$ product of 3.1×10^{11} Hz for the resonator. This result represents an order of magnitude improvement compared with our dielectric resonators. Coupled with the high reflectivity discussed in the previous section, these devices are quite promising for application in future radiation-pressure-based laser cooling experiments.

SUMMARY

We demonstrate high performance monocrystalline optomechanical resonators employing a novel free-free support geometry. Utilizing this updated design, we observe a significant increase in Q, arising from a reduction in clamping-loss mediated mechanical dissipation. Additionally, these structures maintain a reflectivity of at least 99.98% at 1064 nm. With an improved reflectivity and $Q{\cdot}f_r$ product exceeding 10^{11} Hz, these results represent a significant improvement in the performance of optomechanical resonators.

ACKNOWLEDGMENTS

We acknowledge support by the FWF (L426, START), European Commission (MINOS, IQOS), and European Research Council (QOM). G.D.C. is a recipient of a Marie Curie Fellowship and S.G. of a DOC-fellowship of the ÖAW. S.G. and M.R.V. are members of the FWF doctoral program Complex Quantum Systems (W1210).

REFERENCES

[1] M. Aspelmeyer and K. C. Schwab, New J. Phys. 10, 095001 (2008).
[2] T. J. Kippenberg and K. J. Vahala, Science 321, 1172 (2008).
[3] F. Marquardt and S. M. Girvin, Physics 2, 40 (2009).
[4] I. Wilson-Rae, N. Nooshi, W. Zwerger, and T. J. Kippenberg, Phys. Rev. Lett. 99, 093901 (2007).
[5] F. Marquardt, J. P. Chen, A. A. Clerk, and S. M. Girvin, Phys. Rev. Lett. 99, 093902 (2007).
[6] S. Gigan, et al., Nature 444, 67 (2006).
[7] O. Arcizet, et al., Nature 444 71-74 (2006).
[8] S. Gröblacher, J. B. Hertzberg, M. R. Vanner, G. D. Cole, S. Gigan, K. C. Schwab, and M. Aspelmeyer, Nature Phys. 5, 485 (2009).
[9] G. D. Cole, S. Gröblacher, K. Gugler, S. Gigan, and M. Aspelmeyer, Appl. Phys. Lett. 92, 261108 (2008).
[10] Y. A. Akulova, Ph.D. thesis, UC Santa Barbara, 1998.
[11] K. W. Wang, A.-C. Wong, and C. T.-C. Nguyen, J. Microelectromechanical Syst. 9, 347 (2000).
[12] X. H. Huang, X. L. Feng, C. A. Zorman, M. Mehregany, and M. L. Roukes, New J. Phys. 7, 247 (2005).
[13] I. Wilson-Rae, Phys. Rev. B 77, 245418 (2008).
[14] T. Kitano, et al., J. Vac. Sci. Technol. B 15, 167 (1997).
[15] M. C. Huang, Y. Zhou, and C. J. Chang-Hasnain, Nat. Photon. 1, 119 (2007).
[16] E. R. Abraham and E. A. Cornell, Appl. Opt. 37, 1762 (1998).
[17] D. Rugar, H. J. Mamin, and P. Guethner, Appl. Phys. Lett. 55, 2588 (1989).
[18] C. Zener, Phys. Rev. 52, 230 (1937).